Jet-Cooled Phosphorescence Excitation Spectrum of the $T_1(n,\pi^*) \leftarrow S_0$ Transition of 2-Cyclopenten-1-one

Nathan R. Pillsbury,[†] Timothy S. Zwier,[†] Richard H. Judge,[‡] and Stephen Drucker*[,§]

Department of Chemistry, Purdue University, 560 Oval Drive, West Lafayette, Indiana 47907-2084, Department of Chemistry, University of Wisconsin—Parkside, Kenosha, Wisconsin 53141-2000, and Department of Chemistry, University of Wisconsin—Eau Claire, Eau Claire, Wisconsin 54702-2002

Received: March 25, 2007; In Final Form: May 30, 2007

The $T_1(n,\pi^*) \leftarrow S_0$ transition of 2-cyclopenten-1-one (2CP) was investigated by using phosphorescence excitation (PE) spectroscopy in a free-jet expansion. The origin band, near 385 nm, is the most intense feature in the $T_1(n,\pi^*) \leftarrow S_0$ PE spectrum. A short progression in the ring-bending mode (ν'_{30}) is also observed. The effective vibrational temperature in the jet is estimated at 50 K. The spectral simplification arising from jet cooling helps confirm assignments made previously in the room-temperature cavity ringdown (CRD) absorption spectrum, which is congested by vibrational hot bands. In addition to the origin and ν'_{30} assignments, the jet-cooled PE spectrum also confirms the 28^1_0 (C═O out-of-plane wag), 29^1_0 (C═C twist), and 19^1_0 (C═O in-plane wag) band assignments that were made in the $T_1(n,\pi^*) \leftarrow S_0$ room-temperature CRD spectrum. The temporal decay of the T_1 state of 2CP was investigated as a function of vibronic excitation. Phosphorescence from the $v' = 0$ level persists the entire time the molecules traverse the emission detection zone. Thus the phosphorescence lifetime of the $v' = 0$ level is significantly longer than the 2 μs transit time through the viewing zone. Higher vibrational levels in the T_1 state have shorter phosphorescence lifetimes, on the order of 2 μs or less. The concomitant reduction in emission quantum yield causes the higher vibronic bands (above 200 cm^{-1}) in the PE spectrum to be weak. It is proposed that intersystem crossing to highly vibrationally excited levels of the ground state is responsible for the faster decay and diminished quantum yield. The jet cooling affords partial rotational resolution in the $T_1(n,\pi^*) \leftarrow S_0$ spectrum of 2CP. The rotational structure of the origin band was simulated by using inertial constants available from a previously reported density functional (DFT) calculation of the $T_1(n,\pi^*)$ state, along with spin constants obtained via a fitting procedure. Intensity parameters were also systematically varied. The optimized intensity factors support a model that identifies the $S_2(\pi,\pi^*) \leftarrow S_0$ transition in 2CP as the sole source of oscillator strength for the $T_1(n,\pi^*) \leftarrow S_0$ transition.

Introduction

Triplet excited states often play a central role in molecular photochemistry. Low-energy triplet states may be readily populated in a solution-phase environment, via rapid nonradiative relaxation (intersystem crossing) from an initially photoexcited S_1 state.[1] Once the excited system reaches the triplet surface, it is especially prone to chemical reaction, due to a diradical electronic structure and slow radiative decay rate. The return to the ground state typically occurs via $T_1 \rightarrow S_0$ surface hopping that is enhanced in regions where the two states are in close proximity with one another. Thus the T_1 excitation energy, as well as the shape of the triplet potential surface, can strongly influence ground-state product formation. In such cases, characterization of the triplet potential surface is an important step toward understanding or predicting photochemical outcomes.

The computational chemistry community is making significant progress in characterizing excited-state potential surfaces. Improved ab initio[2] and density functional[3,4] methods are making it possible to calculate, with increasing accuracy, the properties of triplet and singlet excited states of medium-sized molecules. In some cases, the accuracy of these excited-state calculations is approaching that of the ground state.

Vibronically resolved spectra provide a rigorous test of computed potential surfaces, via comparison of experimental versus calculated vibrational frequencies, electronic excitation energies, and geometry changes associated with electronic excitation. Comparisons with experiment are critical for refining the computational methods used to treat excited states. Spectroscopic data are routinely obtained for singlet excited states, but the experimental database for triplet excited states is far less well developed—essentially because singlet−triplet transitions originating from the ground state are nominally spin-forbidden. To obtain the crucial experimental benchmarks for testing triplet-state calculations, we have employed the cavity ringdown (CRD)[5] spectroscopic technique in prior studies.[6,7] Here we report continued work, this time using phosphorescence excitation (PE). Both PE and CRD are very sensitive and permit detection of $T_n \leftarrow S_0$ transitions in the gas phase.

We have recently used CRD spectroscopy to investigate $T(n,\pi^*) \leftarrow S_0$ transitions of simple cyclic enones.[6,7] One of these compounds, shown in Figure 1, is 2-cyclopenten-1-one (2CP). Figure 2 shows a CRD spectrum of 2CP recorded at room temperature. This spectrum was obtained previously[7] and is

* To whom correspondence should be addressed. E-mail: druckers@uwec.edu.
[†] Purdue University.
[‡] University of Wisconsin—Parkside.
[§] University of Wisconsin—Eau Claire.

10.1021/jp072353r CCC: $37.00
Published on Web 08/04/2007

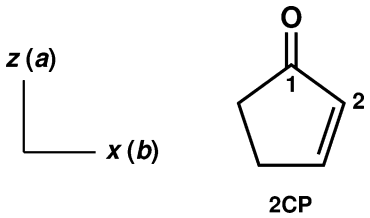

Figure 1. 2-Cyclopenten-1-one, along with coordinate system used in the rotational analysis.

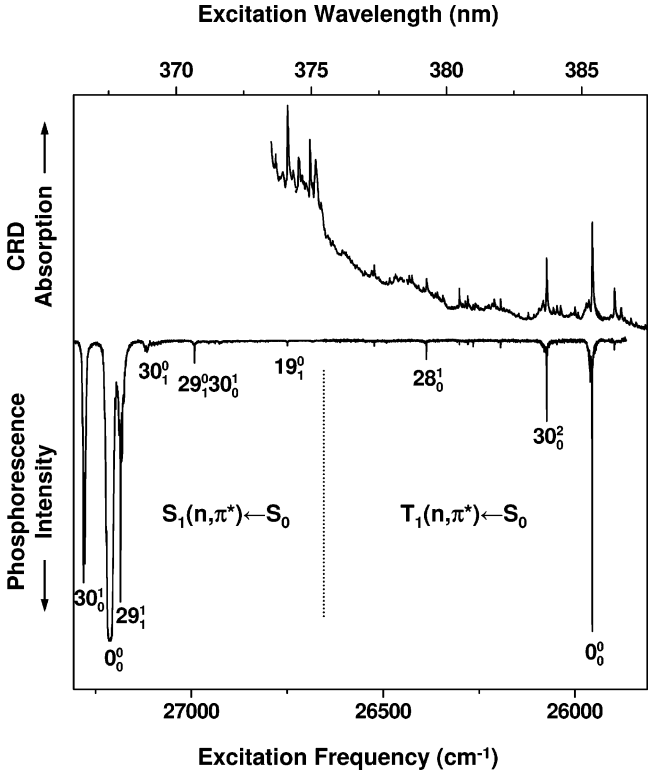

Figure 2. Upper trace: room-temperature cavity ringdown (CRD) spectrum of 2CP vapor (1.6 Torr) contained in a 1 m cell. The spectrum shows the $T_1 \leftarrow S_0$ origin band near 385 nm, a series of singlet−triplet vibronic bands at higher frequencies, and then the onset of $S_1 \leftarrow S_0$ hot-band transitions near 375 nm. This spectrum was recorded previously and is reproduced from ref 7. Lower trace: jet-cooled phosphorescence excitation (PE) spectrum of 2CP. This spectrum is a composite of several single scans recorded over adjacent wavelength regions. The vibronic bands to the left of the dotted line were previously assigned[13] to the $S_1(n,\pi^*) \leftarrow S_0$ system; the bands to the right of the dotted line were previously assigned[7] to $T_1(n,\pi^*) \leftarrow S_0$.

reproduced here to facilitate comparison with the jet-cooled PE spectrum we describe below. The room-temperature spectrum in Figure 2 includes the $T_1(n,\pi^*) \leftarrow S_0$ origin band[8] at 25956 cm^{-1} and spans the region from -150 cm^{-1} to $+850$ cm^{-1} relative to the origin.

Our interest in 2CP stems from a considerable body of computational work on the excited states and photochemistry of the prototype conjugated enone, acrolein (CH_2═CH−CH═O),[9] and its cyclic analogs.[10] The lowest-energy triplet states of these molecules—n,π^* and π,π^*—are involved in much of the photochemistry. For the cyclic enones, the electron configuration and geometry of the prepared triplet state strongly influence the photochemical mechanism and outcome of a given reaction.[11]

The CRD absorption spectrum of 2CP[7] offered the first direct, experimental structural probe of a cyclic enone triplet state. Vibronic analysis of the CRD spectrum provided the $T_1(n,\pi^*)$ excitation energy of 2CP, as well as several fundamental vibrational frequencies in the T_1 state. The vibrational level structure observed for the ring-bending (ν_{30}') mode also made it possible to fit a potential-energy function for this vibration in the T_1 state, to complement experimentally determined ring-bending potentials previously established for the ground[12] and $S_1(n,\pi^*)$[13] states. The $T_1(n,\pi^*)$ excitation energy and vibrational frequencies have been compared to predictions from several computational studies of 2CP.[2a,4]

Vibronic assignments in the $T_1(n,\pi^*) \leftarrow S_0$ CRD spectrum were ascertained by comparison with calculated $T_1(n,\pi^*)$[4] and experimentally known $S_1(n,\pi^*)$[13] vibrational frequencies. Known ground-state combination differences[12] as well as observed deuterium shifts provided a consistency check. However, some uncertainty has remained in the absolute assignments, due to the possibility that a given vibronic band or entire progression in the room-temperature spectrum is built upon a vibrationally excited but unassignable ground-state level. In fact, the large majority of the observed transitions at room temperature must be hot bands (those originating in $\upsilon'' > 0$), as a consequence of the several low-frequency and Franck−Condon active vibrational modes in 2CP.[13]

Hot-band congestion in the room-temperature CRD spectrum has particularly hampered our efforts to characterize the higher-frequency vibrational modes in the $T_1(n,\pi^*)$ state. Starting at a frequency about 500 cm^{-1} above the T_1 origin, vibronic hot bands (shown in the upper trace of Figure 2) associated with the $S_1(n,\pi^*) \leftarrow S_0$ system appear with intensities greater than those of the $T_1(n,\pi^*) \leftarrow S_0$ cold bands. The higher-frequency region of the CRD spectrum (not shown) is congested with $S_1 \leftarrow S_0$ hot bands. Near the S_1 origin ($+1255$ cm^{-1} relative to T_1), these spin-allowed transitions become increasingly intense and preclude observation of any of spin-forbidden $T_1 \leftarrow S_0$ vibronic bands. In particular, it has not been possible to locate the triplet C═C or C═O stretch fundamentals, whose vibronic bands are predicted[4] to be nearly coincident with the $S_1 \leftarrow S_0$ origin band.

The general spectral congestion present in the CRD spectrum has also made it difficult to analyze the rotational contours of the vibronic bands. Such an analysis would be useful for evaluating the accuracy of computed[4] rotational constants. The rotational contours could also offer insight about the singlet excited state or states that contribute oscillator strength to the $T_1(n,\pi^*) \leftarrow S_0$ transition.

Motivated by the desire to (1) confirm our previous vibronic assignments in the $T_1(n,\pi^*) \leftarrow S_0$ CRD spectrum, (2) locate the higher-frequency triplet bands submerged by $S_1(n,\pi^*) \leftarrow S_0$ hot bands, and (3) characterize the rotational contours of the vibronic bands, we undertook to record the $T_1 \leftarrow S_0$ spectrum under supersonic expansion conditions. The cooling obtainable in this environment eliminates nearly all the vibronic hot bands, and further reduces spectral congestion by narrowing the rotational profiles of the observable cold ($\upsilon'' = 0$) bands.

Free-jet expansion, using a pulsed nozzle of circular cross section, provides a convenient and routine way to effect the cooling. However, this experimental arrangement is not ideal for absorption experiments such as CRD, because of a significant sacrifice ($\sim 100\times$) in path length. We thus turned to phosphorescence excitation (PE) spectroscopy. In prior studies of several molecules, PE has been used successfully to record jet-cooled spectra of singlet−triplet transitions involving $\pi^* \leftarrow$ n excitation.[14]

Our choice to pursue PE for T_1 studies of 2CP was also motivated by a previous fluorescence excitation (FE) experiment

on the S_1 state. In 1991 Cheatham and Laane[13] reported the jet-cooled FE spectrum of the $S_1(n,\pi^*) \leftarrow S_0$ band system. The signal-to-noise ratio (S/N) in this experiment was excellent (>1000), despite the characteristically low oscillator strength ($f = 0.0013$)[15] associated with an $\pi^* \leftarrow$ n out-of-plane transition moment. The high quality of the FE spectrum implies that 2CP has an appreciable quantum yield for emission from the $S_1(n,\pi^*)$ state. This characteristic is not shared by homologous molecules such as acrolein[16] or 2-cyclohexen-1-one.[17] Computational studies indicate that for these conformationally flexible enones (where twisting about the C=C bond is permitted), a very fast nonradiative decay path is available from a photoexcited S_1 state to highly vibrationally excited levels of S_0.[9,10] This decay path includes a portion of the $T(n,\pi^*)$ surface, and so the flexible enones might be expected to have negligible phosphorescence quantum yield following triplet excitation. For the more rigid 2CP molecule, in which fluorescence is observed from the $S_1(n,\pi^*)$ state, we expected to observe phosphorescence from the $T_1(n,\pi^*)$ state.

Indeed we found in preliminary *room-temperature* experiments that it was possible to record a $T_1 \leftarrow S_0$ PE spectrum in the origin band region, with comparable S/N to that of the CRD absorption spectrum.[7] To contend with the spin-forbiddenness of the transition, it was necessary to use relatively high laser pulse energies (2−3 mJ) and high photomultiplier gain. Having optimized the experimental conditions for observing phosphorescence in a room-temperature static cell, we initiated the jet-cooled PE experiments presented here.

Experiment Section

The experimental work was carried out at Purdue University, using a free-jet expansion laser-induced fluorescence chamber that is described in detail elsewhere.[18] Briefly, helium was passed through a reservoir heated to about 70 °C, containing a liquid sample of 2CP. The vapor pressure of 2CP at this temperature is 2.7 kPa (20 Torr). The sample was purchased from Acros with a purity of 98% and used without further purification. A pressure of 6 bar helium was applied behind the pulsed valve (General Valve, series 9). A nozzle with 0.8 mm orifice diameter was used. The free-jet expansion was crossed by the frequency-doubled output of a Nd:YAG-pumped tuneable dye laser operating at 20 Hz (~1−1.5 mJ/pulse). Phosphorescence from the sample was collected by two 4 in. mirrors, which focus the collected light through a small (~1 cm) hole in one of the mirrors, via a design similar to that of Majewski et al.[19] and Plusquellic et al.[20] The phosphorescence was collimated, directed through a 400-nm long-pass edge filter (Schott glass), and onto a photomultiplier tube. The photomultiplier output was sent to a digital oscilloscope.

An oscilloscope trace, reproduced in Figure 3, shows the photomultiplier output following excitation of the $T_1 \leftarrow S_0$ origin band. At the beginning of the time profile is a large scattered-light spike. The width of this spike is about 10 ns, reflecting a convolution of the laser pulse shape with the response function of the photomultiplier tube and electronics. The spike is followed by a slow (microsecond-scale) phosphorescence decay, and then a relatively fast dropoff in signal, which is an artifact attributable to the excellent spatial selectivity of the collection mirrors. The molecules are excited at the focal point of the collection optics; as the phosphorescing molecules move away from this point, the efficiency of light collection drops dramatically. This phenomenon caused the emission signal to appear as an essentially flat "shelf" which lasted roughly 2 μs before the fast dropoff took over. This prevented us from determining the phosphorescence lifetime quantitatively.

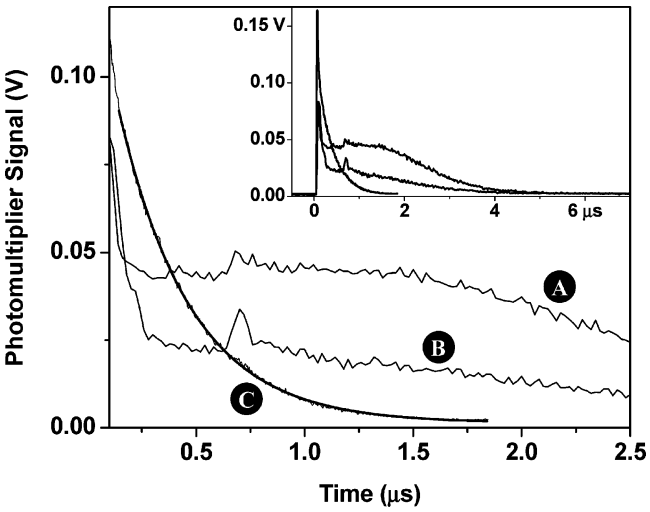

Figure 3. Oscilloscope traces showing emission decay following laser excitation of 2CP. Traces A and B correspond to excitation of the $T_1 \leftarrow S_0$ 0_0^0 and 19_0^1 transitions, respectively. Trace C corresponds to excitation of the $S_1 \leftarrow S_0$ 0_0^0 transition, and was recorded using a lower photomultiplier gain than in A and B. The "spikes" appearing at 0.75 μs in A and B are electronic artifacts attributable to the increased photomultiplier gain. The heavy line in C indicates an exponential fit ($\tau = 330$ ns) to the $S_1 \leftarrow S_0$ fluorescence decay (thin line). The inset shows the oscilloscope traces over a longer time scale; in the case of trace A, this view points out an abrupt loss of emission signal as the phosphorescing molecules travel out of the detector viewing region.

The phosphorescence excitation spectra were recorded by integrating the emission signal over a user-chosen time window. We took advantage of the long T_1 phosphorescence lifetime to discriminate against scattered light and to minimize interference from shorter-lived S_1 excited vibronic states. We typically chose a time window of duration ~1 μs, beginning 500 ns after the laser fired and encompassing the maximum phosphorescence signal. The integrated signal was then plotted against wavelength (or wavenumber) to produce the phosphorescence excitation spectrum.

Results and Discussion

Vibronic Analysis. Figure 2 shows the PE spectrum of 2CP recorded under jet-cooled conditions. The origin band of the $T_1(n,\pi^*) \leftarrow S_0$ transition appears at the low-frequency end of the spectrum. A system of $T_1 \leftarrow S_0$ vibronic bands appears toward higher frequencies, until the $S_1(n,\pi^*) \leftarrow S_0$ origin region is reached at 1255 cm^{-1} relative to the triplet origin. The $S \leftarrow S_0$ bands are identified by their previously determined[13] frequencies. The $S_1 \leftarrow S_0$ bands are also much more intense than those due to the $T_1 \leftarrow S_0$ transition; in fact, the intensity of the $S_1 \leftarrow S_0$ origin band exceeds the dynamic range of our detection system (as configured for phosphorescence measurements), and therefore the singlet origin appears with a distorted band maximum in Figure 2.

In addition to differences in intensity, the rotational band contours distinguish $T_1 \leftarrow S_0$ from $S_1 \leftarrow S_0$ transitions. The $T_1 \leftarrow S_0$ bands are narrower, as a consequence of distinctly different rotational selection rules for singlet versus triplet transitions. The rotational selection rules and band contours are discussed further in the final section of this paper.

Figure 4 compares the room-temperature CRD spectrum with the jet-cooled PE spectrum in the $T_1 \leftarrow S_0$ origin region. The indicated assignments in the room-temperature spectrum are those we ascertained in our previous investigation[7] with the aid of deuterium substitution as well as known ground-state combination differences.

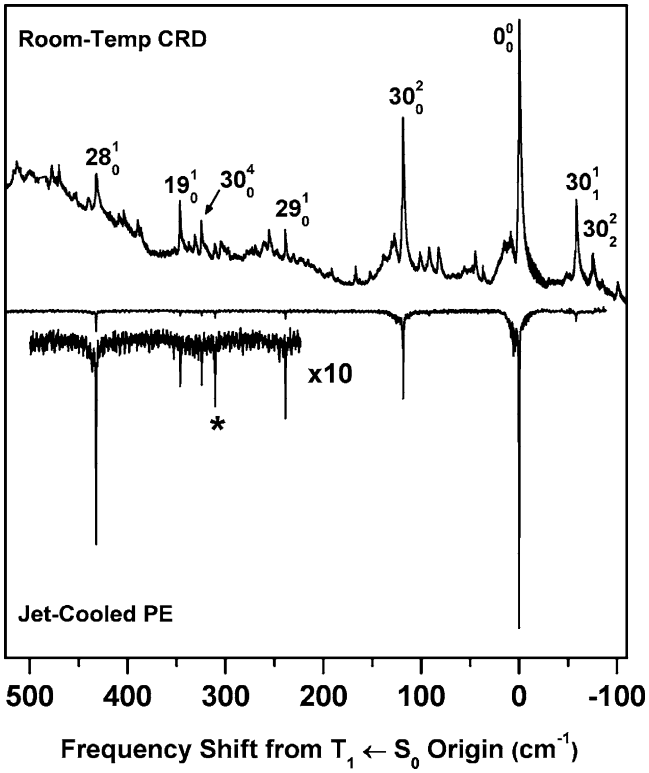

Figure 4. Comparison of the room-temperature CRD spectrum of 2CP (recorded previously)[7] with the present jet-cooled PE spectrum.

As expected, the jet cooling effects a dramatic reduction in spectral congestion. The cold spectrum provides immediate confirmation that the bands originally assigned as 0_0^0 and 30_0^2 (ring-bending excitation) do indeed originate in the zero-point level of the ground state. Both of these bands follow the selection rule $\Delta v_{30} =$ even. This selection rule is applicable because ν_{30} is an out-of-plane mode (a'' symmetry in the C_s point group), and a geometry change occurs along the ν_{30} coordinate[4,7] upon excitation to the T_1 state.

The 30_1^1 transition also follows the symmetry selection rule and is observed in both the CRD and PE spectra. Although the 30_1^1 transition originates in a vibrationally excited level, the fundamental frequency of ν_{30} is only 94 cm^{-1} in the ground electronic state, leading to a Boltzmann factor of 0.64 at room temperature. Thus, the 30_1^1 band appears with appreciable intensity in the room-temperature CRD spectrum. In the ground electronic state, the population of $v_{30} = 1$ diminishes significantly under the vibrational cooling conditions of the jet expansion. Accordingly, the 30_1^1 band is just barely detectable in the jet-cooled PE spectrum. The 30_1^1 to 0_0^0 intensity ratio is 1:30. This ratio depends on the effective vibrational temperature in the jet expansion (T_{vib}) as well as the Franck−Condon factors (FCFs) of the two transitions:

$$\frac{1}{30} = \frac{I(30_1^1)}{I(0_0^0)} = \frac{\mathrm{FCF}(30_1^1)}{\mathrm{FCF}(0_0^0)} \cdot \exp(-\tilde{\nu}_{30}/kT_{vib})$$

From the room-temperature CRD spectrum, $\mathrm{FCF}(30_1^1)/\mathrm{FCF}(0_0^0) \approx 0.5$. This value, when substituted along with $\tilde{\nu}_{30}$ into the above expression, leads to $T_{vib} \approx 50$ K in the present jet expansion. This same temperature of 50 K was reported by Cheatham and Laane[13] in their jet-cooled study of the 2CP $S_1 \leftarrow S_0$ transition, using Ar carrier gas at a stagnation pressure of 2 bar (as compared to 6 bar of He used in the present experiment).

The ν_{30} ring-bending mode of 2CP has significant anharmonicity; this is evident from the nonuniform spacings between the 0_0^0, 30_1^1, 30_2^2, and 30_3^3 sequence members in the room-temperature CRD spectrum (Figure 4). In our previous analysis of that spectrum,[7] the symmetry-allowed 30_1^1 and 30_3^3 bands were particularly useful in characterizing the triplet-state ring-bending potential, as these band positions (together with ground-state combination differences) established the $v'_{30} = 1$ and $v'_{30} = 3$ level energies. In the present jet-cooled investigation, detection of the 30_1^1 band with very low-intensity establishes definitively that it is a hot band and secures its original CRD assignment. This adds further confidence to the ν'_{30} energy-level structure we derived previously for the triplet state, as well as to the fitted ring-bending potential.

In the absence of vibronic interaction the 30_0^1 and 30_0^3 bands are symmetry-forbidden, because the vibrational overlap integral for an out-of-plane mode (a'') vanishes if $\Delta v =$ odd and the molecule remains planar in the excited state. The 30_0^1 and 30_0^3 bands are indeed weak in the CRD spectrum, and their assignments are uncertain due to a congested background. Hence in our previous analysis, we did not rely on the 30_0^1 and 30_0^3 bands to determine the ν'_{30} level energies in the T_1 state. These bands are not observed at all in the present jet-cooled spectrum of the $T_1(n,\pi^*) \leftarrow S_0$ transition.

However, several symmetry-forbidden vibronic bands are observed in the $S_1(n,\pi^*) \leftarrow S_0$ region (Figure 2), including 30_0^1 and 30_1^0. These bands had been observed in previous absorption[21] and fluorescence excitation[13] studies of the $S_1(n,\pi^*) \leftarrow S_0$ band system. The 30_0^1 and 30_1^0 bands are made partially allowed by vibronic mixing of the $S_1(n,\pi^*)$ state, which has A'' symmetry, with an electronic state of A' symmetry—most likely $S_2(\pi,\pi^*)$. In that case, the $S_2(\pi,\pi^*)$ state would carry the oscillator strength for the transition.

A corresponding vibronic mixing is also plausible between the $T_1(n,\pi^*)$ and $T_2(\pi,\pi^*)$ states, and this would lift the $\Delta v_{30} =$ even symmetry restriction in the $T_1(n,\pi^*) \leftarrow S_0$ spectrum. However the $T_2(\pi,\pi^*)$ state would then need to carry the oscillator strength, which is implausible because the $T_2(\pi,\pi^*) \leftarrow S_0$ transition is even more strongly spin-forbidden than the $T_1(n,\pi^*) \leftarrow S_0$.[22] This argument could explain the absence of $\Delta v_{30} =$ odd transitions in the triplet region of the PE spectrum.

Like ν_{30}, the ν_{28} (C═O out-of-plane wag) and ν_{29} (C═C twist) vibrational modes are of a'' symmetry; however, their forbidden $\Delta v = 1$ transitions do appear in the $T_1 \leftarrow S_0$ PE and CRD spectra. Vibronic interaction between $T_1(n,\pi^*)$ and $T_2(\pi,\pi^*)$ is not likely to facilitate observation of such transitions, as implied by the discussion above. It is possible that the 28_0^1 and 29_0^1 bands gain intensity via vibronic interaction within the singlet manifold, involving the singlet state or states to which $T_1(n,\pi^*)$ is coupled by spin−orbit interaction. This type of indirect route has been discussed by Tomer et al.[14c] in their analysis of the $T_1(n,\pi^*) \leftarrow S_0$ PE spectrum of pyrazine.

The appearance of the 28_0^1 and 29_0^1 vibronic bands under jet-cooling conditions has helped us to secure their assignments originally made in the room-temperature $T_1 \leftarrow S_0$ CRD spectrum. Figure 4 shows how the PE spectrum readily picks out the ν'_{28}, ν'_{29}, and ν'_{19} (C═O in-plane wag) triplet-state fundamentals amidst a congested background of unassigned hot bands in the room-temperature CRD spectrum.

The vibronic band labeled * (at 311 cm^{-1} relative to the 25 956 cm^{-1} origin) in Figure 4 appears in both the CRD and PE spectra but was not previously assigned. This band most likely has a $\nu'' = 0$ lower-level assignment, due to its presence

in the jet-cooled PE spectrum. However, we know based on the vibronic analysis above that the unassigned band is neither a fundamental in the $T_1(n,\pi^*)$ state nor part of a low-frequency progression within the $T_1 \leftarrow S_0$ system. As a result, the isolated cold band is tentatively assigned as a member of the strongly forbidden $T_2(\pi,\pi^*) \leftarrow S_0$ band system. In previous computational studies,[10c,23] the $T_2 \leftarrow S_0$ band origin was predicted to be nearly isoenergetic with that of the $T_1 \leftarrow S_0$ system. We therefore tentatively assign the band labeled * at 26 267 cm^{-1} to the $T_2 \leftarrow S_0$ origin band.

Emission Lifetimes and Quantum Yields. Because PE relies on detection of emission, whereas CRD is absorption-based, the patterns of vibronic band intensity differ in the two spectra. For example, although both spectra show a reduced 30_0^2 band intensity compared to the origin (reflecting a decreased Franck−Condon factor), the intensity reduction of 30_0^2 is more severe in the PE spectrum. The other assigned bands in the PE spectrum, at higher frequency, also show a much larger intensity reduction (compared to the origin) than would be predicted from the CRD absorption spectrum. These observations suggest that the phosphorescence quantum yield decreases with increased vibrational excitation in the T_1 state.

This conclusion is also supported by direct observations of phosphorescence lifetime. As indicated in the Experimental section and shown in Figure 3, the lifetime of the T_1 zero-point level significantly exceeds the molecule's ~2 μs transit time through the viewing region of the phosphorescence detection system. However, the lifetimes of the T_1 excited vibronic states are significantly shorter than this. The assigned bands in the 200−500 cm^{-1} region of Figure 4 exhibit phosphorescence decay that is nearly complete by the time the molecules have traversed the detection viewing region. An example is the 19_0^1 band; its phosphorescence decay trace is shown in Figure 3. Quantitative lifetimes are difficult to extract from such data, because the decay of the excited state is convoluted with drop-off in detection efficiency as the molecules travel past the collection optics. However an upper limit for the lifetimes (τ) of these higher-frequency triplet vibronic states is approximately 2 μs, the transit time through the viewing window. This is shorter than the typical radiative lifetime for a $^3(n,\pi^*)$ state.[24] Thus it is plausible that, over the upper range of excitation energies in this experiment, a radiationless decay process is populating a manifold of non-emitting (such as S_0) background states.

A relatively rapid nonradiative decay could explain our difficulties in identifying the triplet-state C═O (ν_5) or C═C stretch (ν_6) vibronic band in the PE spectrum. The 5_0^1 and 6_0^1 bands are both predicted[4] at about 1450 cm^{-1} relative to the $T_1(n,\pi^*) \leftarrow S_0$ origin. They are also expected to have Franck−Condon factors much larger than that of the origin band, based on geometry changes involved in an $\pi^* \leftarrow n$ transition, as well as intensities observed in the $S_1(n,\pi^*) \leftarrow S_0$ absorption spectrum.[21] Nonetheless, we see little evidence of triplet excitation in the PE spectrum at frequencies greater than 26 750 cm^{-1}, or about 800 cm^{-1} above the $T_1 \leftarrow S_0$ origin. Figure 2 shows the higher-frequency region. We do observe the intense $S_1 \leftarrow S_0$ origin band, as well as weaker fundamentals and hot bands attached to it that involve the lowest-frequency vibrational modes. These $S_1 \leftarrow S_0$ vibronic bands congest the PE spectrum, but to a far lesser extent than in the same region of the room-temperature absorption spectrum. Therefore we would expect to observe the 5_0^1 and 6_0^1 bands of the $T_1 \leftarrow S_0$ system in the PE spectrum, unless by coincidence they are submerged by the (relatively sparse) $S_1 \leftarrow S_0$ bands. The absence of intense $T_1 \leftarrow S_0$ bands in this region indicates a dramatically decreased phosphorescence quantum yield for the 5_0^1 and 6_0^1 transitions (compared to the origin), and suggests that the $\upsilon_5' = 1$ and $\upsilon_6' = 1$ states are particularly susceptible to a nonradiative decay process.

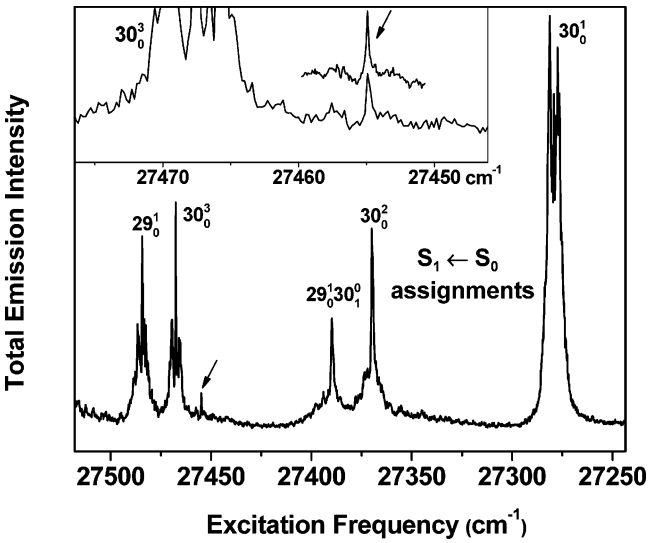

Figure 5. Region of the jet-cooled spectrum of 2CP in which the 5_0^1 (C═O stretch) and 6_0^1 (C═C stretch) vibronic bands are expected for the $T_1 \leftarrow S_0$ transition. This region includes the $S_1 \leftarrow S_0$ band system near its origin (27211 cm^{-1}) and contains several relatively intense singlet bands. The arrow points to a particularly sharp band, at 1499 cm^{-1} above the $T_1 \leftarrow S_0$ origin, that is tentatively assigned as the triplet 5_0^1 or 6_0^1 transition. The inset shows an expanded view of the spectrum and points out a scan of the sharp band recorded using a smaller wavelength step size than in the main spectrum.

We do observe a very weak but comparatively sharp feature at 27 455 cm^{-1} (or 1499 cm^{-1} above the $T_1 \leftarrow S_0$ origin), shown in Figure 5. This feature was not reported in the jet-cooled fluorescence excitation spectrum of the $S_1 \leftarrow S_0$ band system.[13] If the fluorescence excitation study employed a lower scanning resolution than we used here, this sharp feature might not have been detected previously. It is tentatively assigned as the 5_0^1 or 6_0^1 band of the $T_1 \leftarrow S_0$ system.

Computational results of García-Expósito et al.[10c] can help to rationalize the diminished phosphorescence quantum yields in this excitation region. The calculations were aimed at predicting the photophysical fate of conjugated enones following S_1 excitation, but the results do bear on the photophysics of isoenergetic triplet states. The S_1 states were found to have a propensity for decaying nonradiatively through $T(n,\pi^*)$ and $T(\pi,\pi^*)$ intermediates, ultimately reaching highly vibrationally excited S_0 levels. The fastest decay rates were predicted[10c] (and are observed in solution phase)[25] for the more flexible molecules in the series, such as acrolein or 2-cyclohexen-1-one. These two flexible molecules are also found experimentally to have essentially zero quantum yield for S_1 fluorescence in a collisionless environment.[16,26]

The more rigid 2CP molecule has a measurable fluorescence from its S_1 zero-point level (see Figure 3) and phosphorescence from its T_1 zero-point level, so nonradiative processes may be slower in 2CP than in the more flexible enones. Nonetheless the T_1 vibrationally excited levels are short-lived, particularly in the vicinity of the S_1 origin. Thus the nonradiative path $S_1 \rightarrow T(n,\pi^*) \rightarrow T(\pi,\pi^*) \rightarrow S_0$, proposed by García-Expósito et al.[10c], may be at least partially applicable to 2CP. The observed lifetime of the S_1 zero-point level (Figure 3) is approximately 330 ns, shorter than the radiative lifetime of about 1 μs extracted

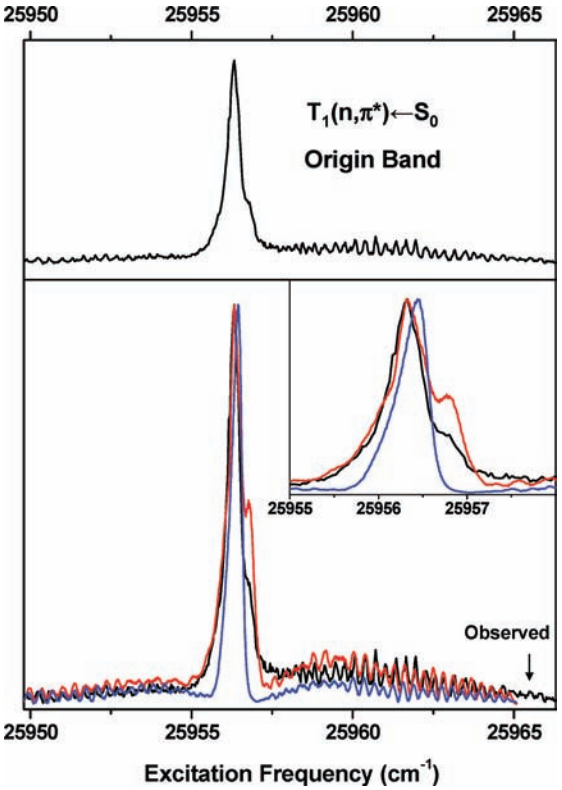

Figure 6. Upper panel: jet-cooled spectrum of the 2CP $T_1 \leftarrow S_0$ origin band, recorded using the highest-resolution scanning increment (0.03 cm^{-1}) permitted with the dye laser system. Lower panel: simulated and observed spectra of the $T_1 \leftarrow S_0$ origin band. The simulation represented by the red trace was conducted using parameter values listed in Table 1, as well as $T_{rot} = 30$ K and $\mu_x = 0$. The blue trace represents the same simulation, but with spin−spin and spin-rotation constants excluded.

from the integrated absorption strength.[15] This observation is consistent with a nonradiative decay process contributing to the measured lifetime. Further studies to elucidate the photophysics following S_1 or T_1 excitation of 2CP would be valuable.

Rotational Analysis. Figure 6 shows the $T_1 \leftarrow S_0$ origin band recorded under jet-cooled conditions, using the highest-resolution scanning increment (0.03 cm^{-1}) permitted with our frequency-doubled dye laser system. The spectral bandwidth (fwhm) of the doubled output (near 385 nm) is estimated to be 0.15−0.20 cm^{-1}.

The spectrum in Figure 6 shows three main structures−a narrow, intense central peak flanked by two broad and much weaker wings. Each wing contains an extended series of resolved features whose maxima are separated by roughly constant (~0.4 cm^{-1}) intervals. Although full rotational resolution is not available under the present experimental conditions, the observed contour and pattern of resolved features broadly indicate the underlying rotational branch structure of this $T_1(n,\pi^*) \leftarrow S_0$ transition. In the discussion below, we outline a model for interpreting the contour and discerning the rotational structure.

The spacing of resolved peaks within the wings ranges from 0.33 to 0.41 cm^{-1}. We may interpret this observation with the aid of calculated inertial constants available from a DFT study of 2CP in its $T_1(n,\pi^*)$ state.[4] The calculation yielded a $\bar{B} = (B + C)/2$ value of 0.0999 cm^{-1} in the T_1 state. In the ground state, the experimental value[27] for $\bar{B}$ is 0.101 cm^{-1}. Thus the resolved rotational features in the spectrum are separated by approximately $4\bar{B}$. A spacing of this magnitude corresponds to the $\Delta N = \pm 2$ (*S*- and *O*-form branch) transitions that are allowed for singlet−triplet vibronic bands. (The *N* quantum number represents total angular momentum excluding electron spin, in a coupling scheme analogous to Hund's case (b) for linear molecules.)

In order to analyze the rotational contour in further detail, we rely on a significant body of previous work on singlet−triplet transitions. Part of this work has focused on rotational selection rules. Hougen, in a seminal treatment, derived the selection rules for rovibronic singlet−triplet transitions of a near-symmetric top.[28] Hougen treated the case of D_{2h} molecules explicitly, and through correlation techniques provided a guide for specifying rotational selection rules for molecules of lower symmetry. Spangler, Pratt, and Birss (SPB) carefully summarized Hougen's results and used them to analyze rotational structure in the jet-cooled $T_1 \leftarrow S_0$ phosphorescence excitation spectrum of glyoxal.[29]

The present $T_1 \leftarrow S_0$ spectrum of 2CP was recorded under conditions similar to that of the glyoxal experiment of SPB. In discussing rotational selection rules as well as line intensities in the present work, we will rely on several conclusions of SPB, with a few modifications to account for the difference in symmetry between glyoxal (C_{2h}) and 2CP (C_s).

Another prior contribution to the interpretation of singlet−triplet spectra takes the form of computer code written by one of us (R.H.J.)[30] and others, notably the unpublished work of F. Birss. The former program[30] was written originally for the purposes of predicting and fitting singlet−triplet spectra of orthorhombic (C_{2v}, D_2, or D_{2h}) asymmetric-top molecules, including cases of large multiplet splittings. For the present work, the program was modified[30b] to include molecules such as 2CP that are of lower symmetry than orthorhombic.

The rotational structure in any $T_1 \leftarrow S_0$ transition ultimately derives from the selection rules between the ground state and the singlet excited-state or states that provide the oscillator strength for the transition. Such singlet states are those having (1) orbitally allowed transitions from the ground state, (2) significant spin−orbit interaction with the T_1 state, and (3) close energy proximity to T_1. For the $T_1(n,\pi^*) \leftarrow S_0$ transition of 2CP, the most significant contributor of oscillator strength is likely to be the $S_2(\pi,\pi^*)$ state. Although the $S_1(n,\pi^*)$ state is closer to $T_1(n,\pi^*)$, the $S_2(\pi,\pi^*)$ state has a much stronger spin−orbit interaction with $T_1(n,\pi^*)$.[31] Moreover, the local symmetry of the $S_1(n,\pi^*) \leftarrow S_0$ transition represents a rotation of charge from the n to the π^* orbital, and so the oscillator strength of this spin-allowed transition is itself very low. Thus the $S_1(n,\pi^*)$ state can be eliminated as a potential contributor of oscillator strength for the $T_1(n,\pi^*) \leftarrow S_0$ transition of 2CP.

These considerations also apply to the case of glyoxal, and the rotational structure in its $T_1 \leftarrow S_0$ spectrum was successfully modeled by SPB[29] under the simplifying assumption that $S_2(\pi,\pi^*)$ is the only radiatively active state coupled to $T_1(n,\pi^*)$. A primary goal of the present analysis is to demonstrate the extent to which this same assumption is applicable to the $T_1(n,\pi^*) \leftarrow S_0$ origin band of 2CP.

For spin-allowed (e.g., singlet−singlet) vibronic bands, the components of the transition dipole moment dictate the rotational selection rules and line strengths and hence determine the type of rotational contour. These same dipole moment components sensitively influence the contour of any singlet−triplet transition that borrows substantial oscillator strength. So to analyze the $T_1(n,\pi^*) \leftarrow S_0$ origin-band contour in 2CP, a starting point is a discussion of the $S_2(\pi,\pi^*) \leftarrow S_0$ transition dipole moment−specifically its components in a molecule-fixed coordinate system.

Our choice of coordinate system is shown in Figure 1. The *z*-axis lies in the plane of the molecule and coincides with the *a* principal axis. (The latter nearly lies nearly along the C=O bond.) The *x*-axis, also in the plane of the molecule, is identified with the *b* principal axis. The *y*-axis is perpendicular to the molecular plane and identified with *c*. This labeling of axes is the same as others[12,13] have used for 2CP and corresponds to a type I^r representation for asymmetric rotors. This representation is compatible with the existing computer code[30a] for simulating the rotational structure in singlet−triplet transitions of asymmetric rotors.

The $S_2(\pi,\pi^*) \leftarrow S_0$ ($A' \leftarrow A'$) transition dipole moment is associated with the conjugated O=C−C=C moiety. The conjugated bond system is oriented approximately in the *z* direction, but the cyclic geometry of 2CP causes the $S_2(\pi,\pi^*) \leftarrow S_0$ transition dipole moment to have both *z* and *x* components. The *y* (out-of-plane) component, which transforms as A'', is zero for the $A' \leftarrow A'$ transition.

In principle, the two dipole moment components of the $S_2(\pi,\pi^*) \leftarrow S_0$ transition (*x* and *z*) could impart intensity to each of three spin sublevels ($|x\rangle$, $|y\rangle$, and $|z\rangle$) of the $T_1(n,\pi^*)$ state. This leads to the possibility that six separate intensity parameters would be needed to model the $T_1 \leftarrow S_0$ spectrum. However we consider only the $|z\rangle$ spin sublevel to be coupled to $S_2(\pi,\pi^*)$, based on arguments of SPB[29] and of Chan and Walton[32] pertaining to spin−orbit interaction in the analogous glyoxal molecule. To model the $T_1 \leftarrow S_0$ origin-band contour of 2CP, we employ two intensity parameters, μ_z and μ_x. These represent the transition dipole integrals that connect the ground state to the $|z\rangle$ sublevel of the triplet state.

We turn next to the singlet−triplet rotational selection rules. Hougen derived four sets of selection rules along with intensity expressions for all ΔK,[33] ΔN, ΔJ allowed transitions. Each set of selection rules applies to a different triplet-state orbital symmetry in the D_{2h} point group. (For four of the eight representations in D_{2h}, the singlet−triplet transition moment is zero.)

In the C_s point group (pertinent to 2CP), the four sets of selection rules coalesce into two sets, one for each irreducible representation (A' and A'') in the group.[28] For the $T_1(n,\pi^*)$ state of 2CP (A''), two groups of transitions are allowed, distinguished by their ΔK selection rule ($\Delta K = 0, \pm 2$ or $\Delta K = \pm 1$). When only the $|z\rangle$ triplet sublevel is considered, the first group of transitions is narrowed to $\Delta K = 0$ and involves the *z* dipole moment operator, whereas the other ($\Delta K = \pm 1$) involves the *x* dipole component.[28] Both groups have allowed $\Delta N = 0, \pm 1, \pm 2$ and $\Delta J = 0, \pm 1$ transitions.

The selection rules and intensity considerations outlined above are incorporated into a computer program we have used to simulate the rotational contour of the 2CP $T_1 \leftarrow S_0$ origin band. An earlier version of the program has been described previously in detail.[30a] That version is applicable to triplet upper states of given symmetry in an orthorhombic (C_{2v}, D_2, or D_{2h}) point group. The program calculates asymmetric-rotor energy levels, including spin−spin and spin-rotation contributions. It then simulates the singlet−triplet spectrum by using the one set of selection rules and line strengths (out of four) that is appropriate for the given triplet-state vibronic symmetry. The present version of the program[30b] deals with molecules of C_s symmetry (such as 2CP) by calculating the energy levels under the higher, orthorhombic symmetry constraints and then superposing two groups of allowed rotational branches ($\Delta K = 0, \pm 2$ and $\Delta K = \pm 1$). To determine the rotational energy levels for our simulations, we used experimental[27] and previously calculated[4] inertial constants for the ground and triplet excited states, respectively.

TABLE 1: Molecular Constants (cm^{-1}) Used to Simulate the $T_1 \leftarrow S_0$ Origin-Band Contour of 2-Cyclopenten-1-one

ground-state inertial constants[a]	
A''	0.24718
B''	0.11963
C''	0.083143
excited-state inertial constants[b]	
A'	0.24824
B'	0.11755
C'	0.082357
spin-rotation constants[c]	
a_0	0.037
a	0.039
spin-spin constants[c]	
α	−0.25
β	−0.25
band origin[c]	
ν_0	25956.29

[a] Experimental values from ref 27. [b] Calculated values from ref 4. [c] Determined from the optimization procedure described in text.

We also used the least-squares fitting feature of the singlet−triplet simulation program, although the spectroscopic data set for the 2CP origin band does not permit determination of genuinely optimized molecular constants. This is because the spectrum was not recorded at high enough resolution to permit assignment of individual ΔK, ΔN, ΔJ rotational transitions. Nonetheless, we did compile a list of the resolved maxima in the wings of the origin band and nominally assigned these to the *O*- and *S*-form rotational transitions expected to be most intense. This enabled us to obtain, through a combination of automated fitting and manual adjustment, sensible estimates of spin constants (a_0, a = spin-molecular rotation interaction constants;[30a,34] and α, β = spin−spin interaction constants)[30a,34] and a band origin. These parameters were fixed during subsequent simulations, while we investigated various possibilities for intensity parameter values (μ_x and μ_z). During this process the inertial constants were held fixed as noted above. The imprecision of the rotational assignments prevented us from determining meaningful centrifugal distortion constants, so none were included in the simulations. Molecular constants used in the simulations are listed in Table 1.

In our investigation we experimented with the relative magnitudes of μ_x and μ_z in order to maximize agreement between simulated and observed spectra. (We also coarsely varied the effective rotational temperature in the jet, in increments of 5 K, until we obtained optimal agreement at $T_{rot} = 30$ K.) Below we show how the chosen μ_x/μ_z ratio affects the simulated band contour and how the optimal choice provides insight about the source of oscillator strength in the $T_1 \leftarrow S_0$ origin-band transition.

We first consider the limiting case of $\mu_x = 0$. This case would hold true if the π-conjugated chromophore in 2CP were aligned exactly with the *a* inertial axis. It is a reasonable starting approximation, considering that the carbonyl moiety is essentially coincident with the *a*-axis, and the alkenyl fragment has a significant component in that direction. Figure 6 (red trace) shows the simulated contour in the $\mu_x = 0$ limit, using $T_{rot} = 30$ K.

The use of a single intensity factor (μ_z) means that the simulated spectrum contains only $\Delta K = 0$ subbands, under the model of intensity borrowing outlined earlier in this section. Among these subbands, the maximum intensity buildup occurs

for the $\Delta N = 0$ (*Q*-form) transitions that comprise that sharp central spike in both the observed and simulated spectra.

Also seen in the simulated spectrum is a secondary maximum on the high-frequency side of the central spike. This appears as a shoulder in the observed spectrum. (The differing intensities of the secondary maximum in the observed vs simulated spectrum can be brought into closer agreement via the μ_x intensity factor, to be discussed below.) The secondary maximum is due to overlapping $\Delta K = 0$, $\Delta N = 0$, $\Delta J = 0$ transitions at large K (>5). It is displaced from the band maximum because of the combined effect of two K-dependences among these *Q*-form branches: (1) the frequency shifts due to spin−spin and spin-rotation interactions[35] are proportional to K^2, and (2) the rotational line strengths[28] are proportional to K^2. The blue trace in Figure 6 supports this interpretation; it shows a simulation with the same parameters as in the red trace, except the spin−spin and spin-rotation constants are set to zero. In the blue trace, the secondary maximum disappears because the $\Delta K = 0$, $\Delta N = 0$, $\Delta J = 0$ branches are not subject to spin splittings. In the red trace, where the secondary maximum does occur, its positions in the observed and simulated spectra agree very well. This agreement supports our choices for spin parameters listed in Table 1.

The red trace in Figure 6 also shows reasonable agreement of the maxima that extend into the high- and low-frequency wings. These features are the $\Delta K = 0$, $\Delta N = +2$ (*S*-form) and $\Delta K = 0$, $\Delta N = -2$ (*O*-form) branches, respectively. The agreement seen within the branches adds confidence to the DFT-calculated values of inertial constants, as well as the spin constants obtained in the optimization procedure described above. The poorer agreement of the blue trace in the wings indicates both the significance of the spin splittings and the reasonably high accuracy with which they have been simulated by the chosen parameters. The level of agreement in both traces diminishes with increasing N', likely attributable to the exclusion of centrifugal distortion constants in the simulation. In a higher resolution experiment, it would likely be possible to obtain a simultaneous fit of both spin and centrifugal distortion constants. Thus the spin constants in Table 1 are better regarded as reasonable starting estimates for such a fit, rather than quantitative determinations on their own.

Next we incorporate the μ_x intensity factor and thereby add $\Delta K = \pm 1$ subbands to the simulated spectrum. Figure 7 shows the effect of increasing the μ_x/μ_z ratio from 0 to 1.5. A prominent change occurs within the central ($\Delta N = 0$, *Q*-form) feature of the simulated spectrum. As μ_x/μ_z increases, the intensity of the secondary maximum decreases and agrees better with that of the shoulder in observed spectrum. This is due to *accumulation* of additional intensity in the main, most central spike, relative to the secondary maximum. The additional intensity comes from $\Delta K = \pm 1$, $\Delta N = 0$ transitions at low K'' (<5). Higher- K'' transitions in the *Q*-form branch are spread out into the wings and have little effect on the high-frequency shoulder of the central maximum.

Thus incorporating the $\Delta K = \pm 1$, $\Delta N = 0$ transitions can bring the central region of the simulated spectrum into good agreement with the observed. Because the $\Delta K = \pm 1$ subbands also contain *S*- and *O*-form ($\Delta N = \pm 2$) branches, it is important also to examine high- and low-frequency wings where the partially resolved $\Delta N = \pm 2$ structure is observed. As seen in Figure 7, increasing the $\Delta K = \pm 1/\Delta K = 0$ intensity ratio in the simulations (by increasing μ_x/μ_z) does not significantly change the maxima positions within the $\Delta N = \pm 2$ branches. That is, the pattern formed by the N quantum number is

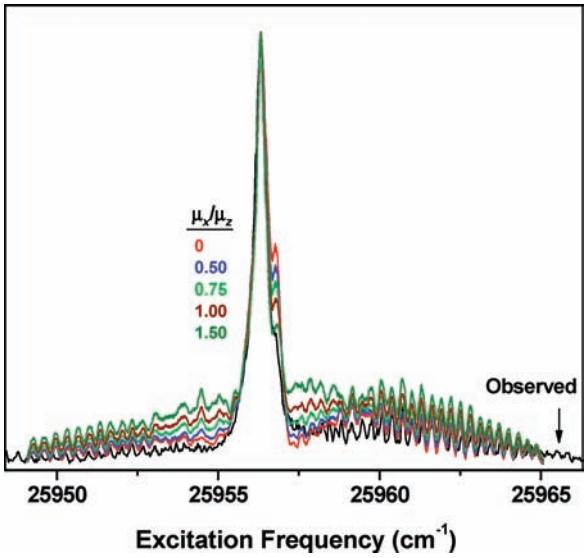

Figure 7. Simulated and observed spectra of the $T_1 \leftarrow S_0$ origin band. Simulations were conducted using parameter values listed in Table 1, in conjunction with the indicated μ_x/μ_z ratios and $T_{rot} = 30$ K.

manifested similarly in both $\Delta K = 0$ and $\Delta K = \pm 1$ subbands. However, when the maximum μ_x/μ_z of 1.5 is used (which affords the best agreement in the central region), the intensities in the wings become unrealistically large. Moreover, a large μ_x/μ_z ratio (>1) in 2CP should be rejected on physical grounds: the $S_2(\pi,\pi^*) \leftarrow S_0$ transition (which presumably supplies the oscillator strength) has a conjugated chromophore that lies more nearly along the $a(z)$ axis than along $b(x)$.

An improved simulation of the origin band would (1) lower intensities in the *O*- and *S*-form branches (2) preserve the shape of the contour in the central region of the band, and (3) rely minimally on a μ_x intensity factor. As discussed above, the $\Delta K = \pm 1$ subbands (stemming from a μ_x intensity factor) appear to be necessary in the simulation for reproducing the relative intensities of the central spike and its shoulder. However, it is possible to retain these subbands without using μ_x exclusively. To do this we relax a constraint imposed earlier in the discussion of intensity borrowing. In that discussion, we assumed that only the $|z\rangle$ triplet sublevel is coupled to the radiatively active $S_2(\pi,\pi^*)$ state. We now put this assumption aside and allow the $|x\rangle$ sublevel to couple to S_2. The resulting mixed spin-orbital state is connected to the ground state by a z transition dipole component;[28] thereby satisfying criterion (3) above. In addition, the orbital symmetry required of the triplet state in this case gives rise[28] to the $\Delta K = \pm 1$ subbands that are apparently required for criterion (2) above.

Therefore as a final step in the simulation, we incorporate an additional intensity parameter, which we name $\mu_z(B_{3g})$, to augment the μ_x and μ_z intensity factors we have been using up to this point. The latter two are renamed as $\mu_x(B_{1g})$ and $\mu_z(B_{1g})$, respectively. The labels in parentheses stem from Hougen's original derivation of the rotational line strengths and refer to the spin symmetry of the triplet sublevel in the D_{2h} point group. In our application to 2CP under C_s symmetry, the three intensity factors $\mu_z(B_{3g})$, $\mu_x(B_{1g})$, and $\mu_z(B_{1g})$ give rise to $\Delta K = \pm 1$, $\Delta K = \pm 1$, and $\Delta K = 0$ subbands, respectively.[28]

Figure 8 shows the simulated origin-band contour, with the ratio of intensity factors $\mu_z(B_{3g}):\mu_x(B_{1g}):\mu_z(B_{1g})$ chosen as 0.5 : 0.5 : 1. In this simulation, the presence of $\Delta K = \pm 1$, $\Delta N = 0$ subbands leads to good agreement in the central region, as was seen earlier (Figure 7, $\mu_x/\mu_z = 1.5$) when the $\mu_z(B_{3g})$ intensity factor was not considered. However, with the $\mu_z(B_{3g})$ parameter

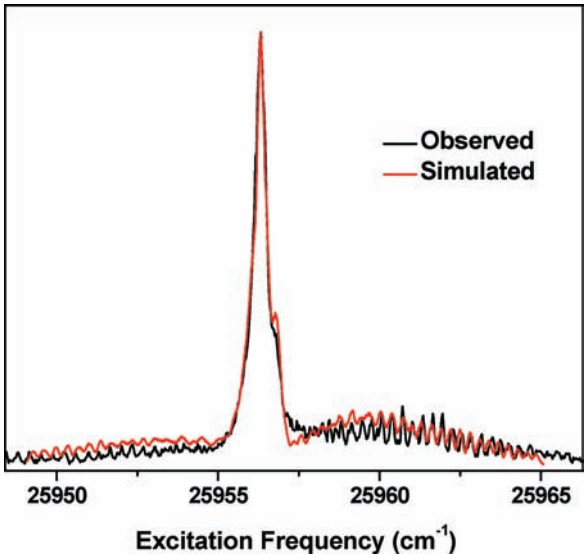

Figure 8. Simulated and observed spectra of the $T_1 \leftarrow S_0$ origin band. Simulations were conducted using parameter values listed in Table 1, with the ratio of intensity factors $\mu_z(B_{3g}):\mu_x(B_{1g}):\mu_z(B_{1g})$ chosen as 0.5:0.5:1 and $T_{rot} = 30$ K.

included as indicated above, the $K = \pm 1$, $\Delta N = \pm 2$ intensities are reduced to zero because the line strength[28] scales as $[\mu_z(B_{3g}) - \mu_x(B_{1g})]$.[2] This affords better agreement between simulated and observed intensities in the wings.

By using the $\mu_z(B_{3g})$ intensity parameter, we consider the $|x\rangle$ sublevel of $T_1(n,\pi^*)$ to couple to the $S_2(\pi,\pi^*)$ state. The magnitude of this spin-orbital interaction is expected to be small but finite for the 2CP molecule. The interaction comes about because the n orbital has a small amount of oxygen p_z character, and so a $|x\rangle$ p_z spin-orbital function of $T_1(n,\pi^*)$ can couple to the π orbital of $S_2(\pi,\pi^*)$. In the limit of C_{2v} symmetry, the n molecular orbital would transform exactly as oxygen p_x, and the spin-orbital interaction with $S_2(\pi,\pi^*)$ would involve only the $|z\rangle$ spin function of the $T_1(n,\pi^*)$ state.

To summarize the rotational analysis, we have shown that it is possible to simulate the $T_1(n,\pi^*) \leftarrow S_0$ origin-band contour of 2CP with reasonably good accuracy by using a model in which the spin-allowed $S_2(n,\pi^*) \leftarrow S_0$ transition is the sole contributor of oscillator strength. In the future, this model can be used to analyze the origin band further if it is recorded at full rotational resolution. The roughly optimized molecular constants obtained in the present simulation (including spin−spin and spin-rotation parameters) can be used as starting points for a fully determined least-squares fit, once rotational assignment of individual ΔK, ΔN, ΔJ rotational transitions is achieved.

In the present simulation, we fixed the triplet-state inertial constants at values obtained from a DFT calculation.[4] The agreement between observed and simulated origin-band contours (Figure 8) adds confidence to the DFT calculated results. Improved agreement of features in the $\Delta N = \pm 2$ wings would presumably be realized by incorporation of centrifugal distortion constants and by calculating the rotational energy levels under non-orthorhombic (e.g., C_s[36]) symmetry constraints. We will undertake such modifications if a fully rotationally resolved spectrum becomes available in the future.

Conclusions

The 2CP molecule is a prototype for understanding the rich photochemistry and photophysics of the cyclic enones. Much of the enone photochemistry is mediated by the lowest-lying triplet states $T(n,\pi^*)$ and $T(\pi,\pi^*)$, and the roles of these states have been probed extensively in prior computational investigations.[11] In our spectroscopic studies of 2CP we are aiming to acquire benchmark structural and dynamical information on the triplet states that can be used to test the accuracy of computational predictions and refine the techniques.

In the present work we have used jet cooling to simplify the vibronically resolved spectrum of the $T_1(n,\pi^*) \leftarrow S_0$ transition. This has enabled us to confirm the vibrational assignments made previously in the room-temperature CRD spectrum.[7] The added confidence in these assignments is important because several of the vibrational fundamentals in the $T_1(n,\pi^*)$ state, as well as the fitted ring-bending potential, differ markedly from those of the $S_1(n,\pi^*)$ state.[7] The differences indicate that the ring is less rigid in the triplet state than in the singlet. As we pointed out in our previous CRD study, this suggests that in the triplet state, the n,π^* chromophore is more delocalized to include the conjugated ring atoms than in the singlet state. The present work, in confirming the triplet vibronic assignments, adds further support to that conclusion.

We have also investigated the lifetimes of the $T_1(n,\pi^*)$ vibronic states. We observe a pronounced shortening of the phosphorescence lifetime at higher vibrational energy, particularly around 1200 cm^{-1}, the region of the $S_1(n,\pi^*) \leftarrow S_0$ origin. We attribute the faster decay in this region to nonradiative relaxation to the ground state. This nonradiative decay has been invoked in previous computational[10] and solution-phase experimental[25] investigations of enone photochemistry. The present work constitutes the first state-resolved investigation of this decay. Our findings set the stage for a jet-cooled CRD absorption study that could characterize the lifetimes more precisely via measurements of homogeneous line broadening.

Finally, the jet cooling has enabled us to record the $T_1(n,\pi^*) \leftarrow S_0$ origin-band rotational profile without congestion from high-J'' states or interference from vibrational hot bands. We were able to simulate the rotational contour by using a model in which the $S_2(\pi,\pi^*) \leftarrow S_0$ transition provides the oscillator strength. This modeling process is an important step toward a comprehensive spectroscopic characterization of the $T_1(n,\pi^*)$ state. The next step is to record the $T_1(n,\pi^*) \leftarrow S_0$ spectrum at high resolution, so that the triplet-state molecular constants can be determined quantitatively by least-squares fitting. This goal has been achieved for just a handful of medium-sized organic molecules (notably glyoxal,[29] acetaldehyde,[14b] and pyrazine).[14c,d] The 2CP molecule, with its cyclic enone functionality, would be a uniquely valuable addition to this list.

Acknowledgment. Acknowledgment is made by S.D. to the Donors of The Petroleum Research Fund (42824-B6), administered by the American Chemical Society, for partial support of this research. S.D. also gratefully acknowledges funding from the National Science Foundation (CHE-0517879), as well as sabbatical travel support from the Office of Research and Sponsored Programs of the University of Wisconsin-Eau Claire.

References and Notes

(1) (a) Wayne, R. P. *Principles and Applications of Photochemistry*; Oxford University Press: Oxford, 1988; pp 86−90. (b) Turro, N. J. *Modern Molecular Photochemistry*; Benjamin/Cummings: Menlo Park, CA, 1978; pp 185−188. (c) Klessinger, M.; Michl, J. *Excited States and Photochemistry of Organic Molecules*; VCH: New York, 1995; pp 254−256.

(2) See, for example: (a) Grimme, S.; Izgorodina, E. *Chem. Phys.* **2004**, *305*, 223. (b) Dreuw, A.; Head-Gordon, M. *Chem. Rev.* **2005**, *105*, 4009. (c) Chang, J. L. *J. Chem. Phys.* **2005**, *122*, 194321. (d) Pugliesi, I; Muller-Dethlefs, K. *J. Phys. Chem. A* **2006**, *110*, 13045. (e) Chaudhuri, R. K.; Krishnamachari, S. L. N. G.; Freed, K. F. *J. Mol. Struct. (THEOCHEM)* **2006**, *768*, 119. (f) Chang, J. L.; Tsao, C. W. *Chem. Phys. Lett.* **2006**, *428*, 23.

(3) See, for example: (a) Furche, F.; Ahlrichs, R. *J. Chem. Phys.* **2002**, *117*, 7433. (b) Casadesus, R.; Vendrell, O.; Moreno, M.; Lluch, J. M. *Chem. Phys. Lett.* **2005**, *405*, 187. (c) Scalmani, G.; Frisch, M. J.; Mennucci, B.; Tomasi, J.; Cammi, R.; Barone, V. *J. Chem. Phys.* **2006**, *124*, 094107.

(4) Choo, J.; Kim, S.; Drucker, S.; Laane, J. *J. Phys. Chem. A* **2003**, *107*, 10655.

(5) (a) O'Keefe, A.; Deacon, D. A. G. *Rev. Sci. Instrum.* **1988**, *59*, 2544. (b) Scherer, J. J.; Paul, J. B.; O'Keefe, A.; Saykally, R. J. *Chem. Rev.* **1997**, *97*, 25.

(6) Drucker, S.; Van Zanten, J. L.; Gagnon, N. D.; Gilles, E. J.; Pillsbury, N. R. *J. Mol. Struct.* **2004**, *692*, 1.

(7) Pillsbury, N. R.; Choo, J.; Laane, J.; Drucker, S. *J. Phys. Chem. A* **2003**, *107*, 10648.

(8) In ref 7 we reported the wavenumber of the origin band maximum as 25963.55(7) cm^{-1}. This value is incorrect because we inadvertently neglected to convert calibrated air wavelengths to vacuum. By carrying out the conversion, we obtain a wavenumber value of 25956.33(7) cm^{-1} that is used in the present work.

(9) (a) Reguero, M.; Olivucci, M.; Bernardi, F.; Robb, M. A. *J. Am. Chem. Soc.* **1994**, *116*, 2103. (b) Bernardi, F.; Olivucci, M.; Robb, M. A. *Pure Appl. Chem.* **1995**, *67*, 17. (c) Fang, W.-H. *J. Am. Chem. Soc.* **1999**, *121*, 8376.

(10) (a) Broeker, J. L.; Eksterowicz, J. E.; Belk, A. J.; Houk, K. N. *J. Am. Chem. Soc.* **1995**, *117*, 1847. (b) Wilsey, S.; González, L.; Robb, M. A.; Houk, K. N. *J. Am. Chem. Soc.* **2000**, *122*, 5866. (c) García-Expósito, E.; Bearpark, M. J.; Ortuño, R. M.; Branchadell, V.; Robb, M. A.; Wilsey, S. *J. Org. Chem.* **2001**, *66*, 8811. (d) García-Expósito, E.; Bearpark, M. J.; Ortuño, R. M.; Robb, M. A.; Branchadell, V. *J. Org. Chem.* **2002**, *67*, 6070.

(11) (a) Reguero, M.; Olivucci, M.; Bernardi, F.; Robb, M. A. *J. Org. Chem.* **1997**, *62*, 6897. (b) Zimmerman, H. E.; Nesterov, E. E. *J. Am. Chem. Soc.* **2002**, *124*, 2818. (c) Zimmerman, H. E.; Nesterov, E. E. *J. Am. Chem. Soc.* **2003**, *125*, 5422.

(12) Chao, T. H.; Laane, J. *J. Mol. Spectrosc.* **1973**, *48*, 266.

(13) Cheatham, C. M.; Laane, J. *J. Chem. Phys.* **1991**, *94*, 5394.

(14) See, for example: (a) Ottinger, C.; Winkler, T *Chem. Phys. Lett.* **1999**, *314*, 311. (b) Liu, H.; Lim, E. C.; Muñoz-Caro, C.; Niño, A.; Judge, R. H.; Moule, D. C. *J. Chem. Phys.* **1996**, *105*, 2547. (c) Tomer, J. L.; Holtzclaw, K. W.; Pratt, D. W.; Spangler, L. H. *J. Chem. Phys.* **1988**, *88*, 1528. (d) Holtzclaw, K. W.; Spangler, L. H.; Pratt, D. W. *Chem. Phys. Lett.* **1988**, *161*, 347. (e) Moule, D. C.; Sharp, A. C.; Judge, R. H.; Liu, H.; Lim, E. C. *J. Chem. Phys.* **1998**, *108*, 1874. (f) Ottinger, C.; Vilesov, A. F.; Winkler, T. *Chem. Phys. Lett.* **1993**, *208*, 299.

(15) The oscillator strength for the $S_1(n,\pi^*) \leftarrow S_0$ transition in 2CP was estimated from a room-temperature absorption spectrum of the vapor recorded by using a spectrophotometer. The ϵ_{max} value (75 $dm^3\ mol^{-1}\ cm^{-1}$), combined with the half-width of the absorption band (4000 cm^{-1}), provides an estimate of integrated absorption strength, leading to an oscillator strength (Turro, N. J. *Modern Molecular Photochemistry*; Benjamin/Cummings: Menlo Park, CA, 1978; pp 86−90) of 0.0013.

(16) Paulisse, K. W.; Friday, T. O.; Graske, M. L.; Polik, W. F. *J. Chem. Phys.* **2000**, *113*, 184.

(17) Gilles, E. J.; Choo, J.; Autrey, D.; Rishard, M.; Drucker, S.; Laane, J. *Can. J. Chem*. **2004**, *82*, 867.

(18) Pillsbury, N. R.; Plusquellic, D. F.; Meerts, W. L.; Zwier, T. S. Manuscript in preparation.

(19) (a) Majewski, W. A.; Meerts, W. L. *J. Mol. Spectrosc.* **1984**, *104*, 271. (b) Majewski, W. A.; Plusquellic, D. F.; Pratt, D. W. *J. Chem. Phys.* **1989**, *90*, 1362.

(20) Plusquellic, D. F.; Davis, S. R.; Jahanmir, F. *J. Chem. Phys*. **2001**, *115*, 225.

(21) Gordon, R. D.; Orr, D. R. *J. Mol. Srectrosc.* **1988**, *129*, 24.

(22) Turro, N. J. *Modern Molecular Photochemistry*; Benjamin/Cummings: Menlo Park, CA, 1978; pp 105−109.

(23) (a) Froese, R. D. J.; Morokuma, K. *Chem. Phys. Lett.* **1996**, *263*, 393. (b) Sunoj, R. B.; Lakshminarasimhan, P.; Ramamurthy, V.; Chandrasekhar, J. *J. Comput. Chem.* **2001**, *22*, 1598.

(24) Turro, N. J. *Modern Molecular Photochemistry*; Benjamin/Cummings: Menlo Park, CA, 1978; p 121.

(25) Ref 10c cites transient absorption measurements of triplet-state lifetimes in solution. The decay of the S_1 state is proposed to proceed through a bottleneck $T(\pi,\pi^*)$ state that is coupled to S_0.

(26) Laane, J. Personal communication.

(27) Ruoff, R.; Krebs, A.; Schaeffler, T.; Stiegler, G.; Bodenseh, H. K. *J. Mol. Struct*. **1997**, *407*, 93.

(28) Hougen, J. *Can. J. Phys.* **1964**, *42*, 433.

(29) Spangler, L. H.; Pratt, D. W.; Birss, F. W. *J. Chem. Phys*. **1986**, *85*, 3229.

(30) (a) Judge, R. H.; Korale, A. A.; York, J. J.; Joo, D.-L.; Clouthier, D. J.; Moule, D. C. *J. Chem. Phys*. **1995**, *103*, 5343. (b) Judge, R. H.; Kodet, J. *Comput. Phys. Comm*. [Early online access]. DOI: 10.1016/j.cpc.2007.02.094.

(31) Klessinger, M.; Michl, J. *Excited States and Photochemistry of Organic Molecules*; VCH: New York, 1995; pp 29−30.

(32) Chan, I. Y; Walton, K. R.; *Mol. Phys.* **1977**, *34*, 65.

(33) Because 2CP is a nearly prolate asymmetric rotor, the label K_a should technically be used instead K in specifying rotational energy levels and selection rules. (K_a becomes the good quantum number K in the exact prolate limit.) For simplicity of notation, we use the symbol K as a substitute for K_a in the discussion of rotational selection rules.

(34) Van Vleck, J. H. *Rev. Mod. Phys.* **1951**, *23*, 213.

(35) Herzberg, G. *Molecular Spectra and Molecular Structure: Electronic Spectra and Electronic Structure of Polyatomic Molecules*; Krieger: Malabar, FL, 1991; Vol. III, p 90.

(36) In Ref. 7 we determined that the ring-bending (ν_{30}) potential has a small (43 cm^{-1}) barrier to planarity in the T_1 state. The zero-point level of this vibration is about 20 cm^{-1} below the barrier to planarity. Hence the $\nu' = 0$ upper state of the origin-band transition technically does not have a planar vibrationally averaged geometry. The most accurate calculation of rotational energy levels would thus be accomplished by lifting even the C_s symmetry restriction.